Atomic depth distribution and effects of surfactants in growth of Ag and Au on Si(111)-$\sqrt{3}\times\sqrt{3}$-Ga(1ML), -4×1-In and $-2\sqrt{3}\times2\sqrt{3}$-Sn surfaces at room temperature

T. Yamanaka*
Catalysis Research Center, Hokkaido University, Sapporo 060-0811, Japan

S. Ino
Department of Electronics, Faculty of Engineering, Utsunomiya University, Utsunomiya, 321-8585, Japan

(Received 9 January 2002; revised manuscript received 18 April 2002; published 19 August 2002)

The atomic depth distribution and growth modes in six growth processes, the growth of Ag and Au on $\sqrt{3}\times\sqrt{3}$-Ga(1 ML), 4×1-In, and $2\sqrt{3}\times2\sqrt{3}$-Sn surfaces, were studied at room temperature by using reflection high-energy electron diffraction and characteristic x-ray measurements as functions of glancing angle θ_g of the incident electron beam. In all growth processes, intermixing between a preadsorbed metal [metal *A*, (Ga, In, Sn)] and a grown metal [metal *B* (Ag, Au)] was observed after deposition of 1 ML of metal *B*. During further deposition of metal B, three growth modes were observed: (i) further intermixing between metal *A* and metal *B* (Ag/In and Ag/Sn), (ii) segregation of metal *A* to the uppermost layers (Ag/Ga, Au/Ga), and (iii) segregation of a part of metal *A* to the uppermost layers and intermixing of the other part of metal *A* with metal *B* (Au/In, and Au/Sn). In all processes, metal *A* acted as a surfactant, i.e., the surface roughness was suppressed by preadsorption of metal *A*, resulting in a layer-by-layer growth mode of metal *B*.

DOI: 10.1103/PhysRevB.66.085316 PACS number(s): 81.15.−z, 61.14.Hg, 68.55.−a

I. INTRODUCTION

Much interest has recently been shown in the control of the growth of metals on semiconductors and in a characterization of the resultant structures, since these subjects are related to the fabrication of nanomaterials with interesting functions. In the future, devices with high performance will be designed on a nanometer scale, and techniques for growing high-quality metal films with thicknesses of several atomic layers will be required.

Surfactant-mediated epitaxy (SME) has been extensively used for altering the growth mode to fabricate uniform-layer structures with few defects. By using this technique, the growth mode changes from a Stranski-Krastanov mode to a layer-by-layer mode by preadsorption of surfactant atoms on the substrate. During these growth processes, the surfactant always moves to the uppermost layer. Although the technique of SME has been used in many growth processes of a semiconductor on a semiconductor and a metal on a metal,[1–3] there have been only a few reports on the application of SME to growth processes of metals on semiconductor surfaces,[4–6] despite the importance of metal/semiconductor systems for technical reasons.

In this paper, growth modes in six growth processes—growth of Ag and Au on Si(111)-$\sqrt{3}\times\sqrt{3}$-Ga (1 ML), 4×1-In, and $2\sqrt{3}\times2\sqrt{3}$-Sn surfaces—are described. The morphology of grown films was analyzed by reflection high-energy x-ray diffraction (RHEED), and the atomic depth distribution of elements was determined by measuring characteristic x rays excited by a RHEED beam, both as functions of incident glancing angle θ_g. In all growth processes, intermixing between a preadsorbed metal [metal *A* (Ga, In, Sn)] and a grown metal [metal *B* (Ag, Au)] occurred after deposition of 1 ML of metal *B*. For further deposition of metal *B*, growth modes were classified into three types: (i) further intermixing (Ag/In and Ag/Sn), (ii) segregation of metal *A* to the uppermost layers (Ag/Ga, Au/Ga), and (iii) segregation of a part of metal *A* to the uppermost layers and mixing of the other part of metal *A* with metal *B* (Au/In, and Au/Sn). In all processes, metal *A* acted as a surfactant, resulting in a layer-by-layer growth mode and formation of flat films of metal *B*.

II. EXPERIMENT

In this study, surface structures during growth processes were monitored by RHEED observation. Simultaneously, atomic depth distribution was analyzed from the θ_g dependence of intensities of characteristic x rays emitted from the surfaces excited by the RHEED beam.[7] The resolution of depth in this method is 1 ML for the uppermost layers and several ML's for deeper regions. In addition, this method is useful for analyzing the growth processes of films, even films that consist of fine particles and liquid or amorphous structures, as well as the growth processes of single crystals. In general, x-ray spectroscopy is not surface sensitive since a significant amount of x rays from deep regions is detected. However, signals from deep regions can be reduced, and x-ray spectroscopy becomes a surface-sensitive method when the x-ray detector is placed at an angle near the critical angle for total reflection,[8,9] a technique called total reflection angle x-ray spectroscopy-(TRAXS).[9] This technique was used in the present study. The details of the apparatus used in the present work was described in a previous paper.[10] To optimize θ_t smoothly, an x-ray detector with a slit was mounted on a stage on a fulcrum, which is 40 cm away from the sample. θ_t was changed by tilting the stage to shift the detector up and down. The width of the take-off angle was 0.4°, and it was set in the range of 0.5–0.9°. A small electron gun on a turntable was then rotated around an axis lying on the sample surface in the ultrahigh-vacuum (UHV) chamber,

 ©2002 The American Physical Society

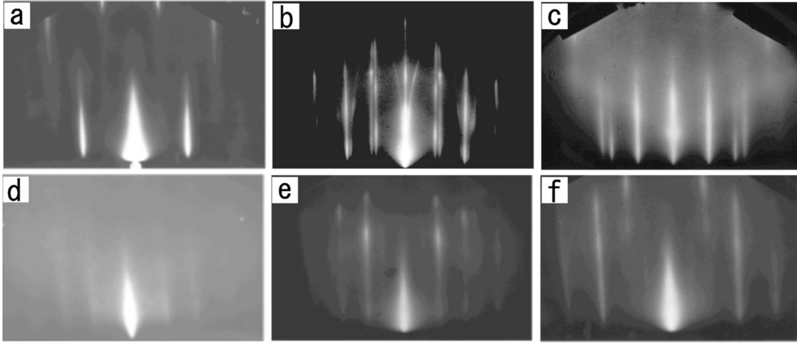

FIG. 1. RHEED patterns taken during growth processes of Ag and Au on Si(111)-$\sqrt{3}\times\sqrt{3}$-Ga (1 ML), 4×1-In, and $2\sqrt{3}\times2\sqrt{3}$-Sn surfaces at room temperature. (a) Ag(15 ML)/$\sqrt{3}\times\sqrt{3}$-Ga (1 ML). (b) Ag (6 ML)/4×1-In. (c) Ag (5 ML)/$2\sqrt{3}\times2\sqrt{3}$-Sn. (d) Au(3 ML)/$\sqrt{3}\times\sqrt{3}$-Ga (1 ML). (e) Au (10 ML)/4×1-In. (f) Au (5 ML)/$2\sqrt{3}\times2\sqrt{3}$-Sn. All patterns show streaks, indicating that grown films were flat.

and the positions of the sample and the detector were fixed. The glancing angle θ_g could be changed from 0 to 180°, with an angular resolution of 0.036°, by using a stepping motor. The electron gun was operated at an acceleration voltage of 10 keV for the growth of Ag and Au on 4×1-In and $2\sqrt{3}\times2\sqrt{3}$-Sn, while a voltage of 15 keV was used for the growth of Ag and Au on $\sqrt{3}\times\sqrt{3}$-Ga (1 ML), since excitation of GaK characteristic x-rays requires a higher electron energy. The x rays emitted from the sample surface propagated successively, through the first beryllium window for the UHV seal, 5 mm of air, and the second beryllium window of the vacuum seal of solid state detector, finally reaching the Si (Li) detector. The base pressure in the chamber was 1×10^{-10} Torr, and the working pressure was always around 5×10^{-10} Torr. The sample was cut in a circular shape of 12 mm in diameter from a mirror-polished Si(111) wafer. Cleaning of the Si(111) surface was performed by heating above 1200° C by electron bombardment until a clear 7×7 RHEED pattern was observed. Si(111)-$\sqrt{3}\times\sqrt{3}$-Ga (1 ML), 4×1-In, and $2\sqrt{3}\times2\sqrt{3}$-Sn structures were prepared by deposition of metals from coiled tungsten filaments.

III. RESULTS

A. RHEED observation

The following three kinds of metal-precovered Si(111) surface were prepared. (i) Si(111)-$\sqrt{3}\times\sqrt{3}$-Ga (1 ML): Si(111)-$\sqrt{3}\times\sqrt{3}$-Ga was formed by a 1/3 ML of Ga deposition on an Si(111)-7×7 clean surface at 500° C.[11] This surface was cooled to room temperature, and 2/3 ML of Ga was then deposited. At this stage, the total coverage of Ga was 1 ML. The RHEED pattern of this surface showed streaks of a $\sqrt{3}\times\sqrt{3}$ structure.[4] (ii) Si(111)-4×1-In surface: 1 ML of In was deposited on an Si(111)-7×7 surface at 500° C,[12] and the surface was cooled to room temperature. (iii) Si(111)-$2\sqrt{3}\times2\sqrt{3}$-Sn surface: 1 ML of Sn was deposited on an Si(111)-7×7 surface at 500° C,[13] and then the surface was cooled to room temperature.

Ag or Au was then deposited on these surfaces at room temperature, and morphology of films during growth was studied by RHEED observation. Figures 1(a)–1(f) show RHEED patterns during these six growth processes: (a)–(f) are results for Ag(15 ML)/$\sqrt{3}\times\sqrt{3}$-Ga (1 ML), Ag (6 ML)/4×1-In, Ag(5 ML)/$2\sqrt{3}\times2\sqrt{3}$-Sn, Au(3 ML)/$\sqrt{3}\times\sqrt{3}$-Ga (1 ML), Au(10 ML)/4×1-In and Au (5 ML)/$2\sqrt{3}\times2\sqrt{3}$-Sn, respectively. Each pattern showed nearly vertical streaks, indicating that the grown film was flat.

B. θ_g dependencies of x-ray emission

1. Growth of Ag on a Si(111)-$\sqrt{3}\times\sqrt{3}$-Ga(1 ML) surface

θ_g dependencies of GaK, AgL and SiK characteristic x rays measured during growth of Ag on an Si(111)-$\sqrt{3}\times\sqrt{3}$-Ga (1 ML) surface are shown in Fig. 2. Since the diameters of the incident electron beam and the sample were about 0.15 and 12 mm, respectively, the entire beam fell on the sample at θ_g above 0.7°. The rapid decreases in x-ray yields below 0.7° are due to the finite size of the sample.

At an Ag coverage of 1 ML ($\Theta_{Ag}=1$), θ_g dependencies of GaK and AgL had maxima at 1°, and decreased above $\theta_g=1°$ with increases in θ_g, as shown in Fig. 2(a). The

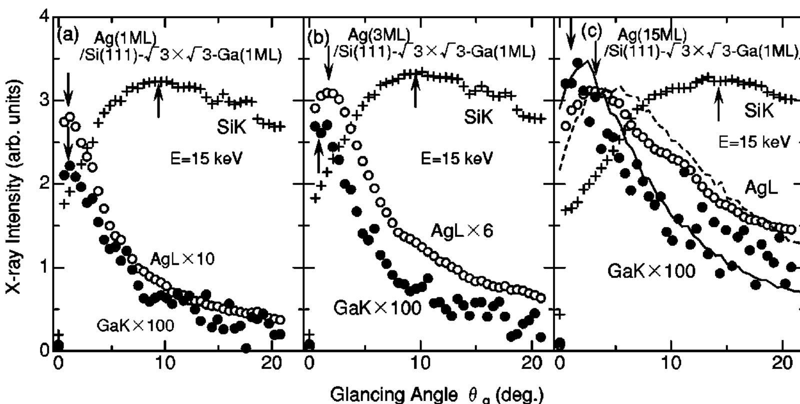

FIG. 2. θ_g dependencies of characteristic x rays, SiK, AgL, and GaK, taken during growth of Ag on an Si(111)-$\sqrt{3}\times\sqrt{3}$-Ga (1 ML) surface at room temperature. (a), (b), and (c) show results at $\Theta_{Ag}=1, \Theta_{Ag}=3$, and $\Theta_{Ag}=15$, respectively. Peak positions of the θ_g dependencies are indicated by arrows. Solid and dashed curves are θ_g dependencies calculated by Monte Carlo simulation, assuming depth distribution of metals with model (a) in Fig. 6. Detailed distribution of metals is described in the text.

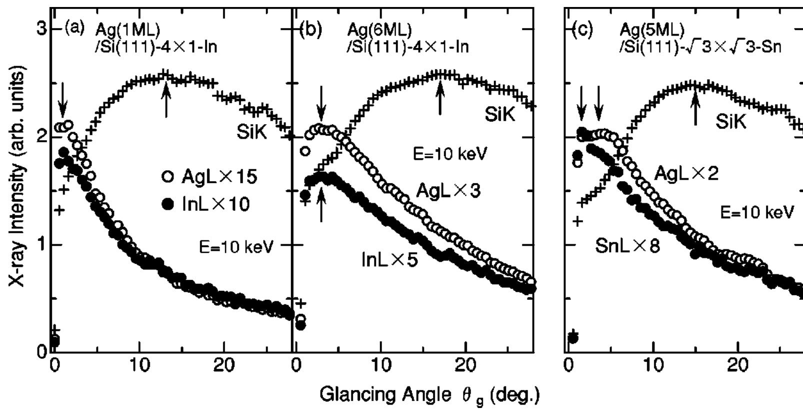

FIG. 3. (a) and (b) show θ_g dependencies of characteristic x rays, SiK, AgL, and InL, taken during growth of Ag on an Si(111)-4×1-In surface at room temperature, at $\Theta_{Ag}=1$ and $\Theta_{Ag}=6$, respectively. (c) θ_g dependencies of characteristic x rays SiK, AgL, and SnL, taken during growth of Ag on an Si(111)-$2\sqrt{3}\times 2\sqrt{3}$-Sn surface at room temperature at $\Theta_{Ag}=5$. Peak positions of the θ_g dependencies are indicated by arrows.

shapes of these two θ_g dependencies are very similar. On the other hand, θ_g dependence of SiK had a broad maximum at 9°. At $\Theta_{Ag}=3$, the maximum of GaK was still observed at 1°, while that of AgL shifted to 2° as shown in Fig. 2(b). At $\Theta_{Ag}=15$, the peaks of AgL shifted to 3°, but, that of GaK still existed at 1°, as shown in Fig. 2(c). The peak of SiK also shifted to higher θ_g with increases in Θ_{Ag} from 9° [Fig. 2(a)] to 14° [Fig. 2(c)].

2. Growth of Ag on Si(111)-4×1-In and $2\sqrt{3}\times 2\sqrt{3}$-Sn surfaces

Figure 3(a) shows θ_g dependencies of InL, AgL and SiK emissions after 1 ML of Ag deposition on an Si(111)-4×1-In surface. Behaviors of InL and AgL were very similar, show ing peaks at 1° and rapid decreases above 1°. After further deposition of 5 ML of Ag ($\Theta_{Ag}=6$), the maxima of InL and AgL shifted to 2.5°, and θ_g dependencies of InL and AgL were still very similar, as shown in Fig. 3(b). The peak of SiK shifted from 13° to 17° as Θ_{Ag} increased from 1 to 6 as shown in Figs. 3(a) and 3(b).

Similar θ_g dependencies were observed during growth of Ag on an Si(111)-$2\sqrt{3}\times 2\sqrt{3}$-Sn surface. Figure 3(c) shows the results at $\Theta_{Ag}=5$. The θ_g dependencies of SnL and AgL were similar, although the peak of SnL (1.5°) was found at lower θ_g than that of AgL (3°). The θ_g dependence of SiK showed a broad peak at 15°.

3. Growth of Au on Si(111)-$\sqrt{3}\times\sqrt{3}$-Ga (1 ML), 4×1-In, and $2\sqrt{3}\times 2\sqrt{3}$-Sn surfaces

Figures 4(a) and 4(b), 4(c) and 4(d), and 4(e) and 4(f) show θ_g dependencies of characteristic x-ray emissions measured during growth of Au on Si(111)-$\sqrt{3}\times\sqrt{3}$-Ga (1 ML), 4×1-In, and $2\sqrt{3}\times 2\sqrt{3}$-Sn surfaces, respectively. These results are similar to those of growth of Ag on the Si(111)-

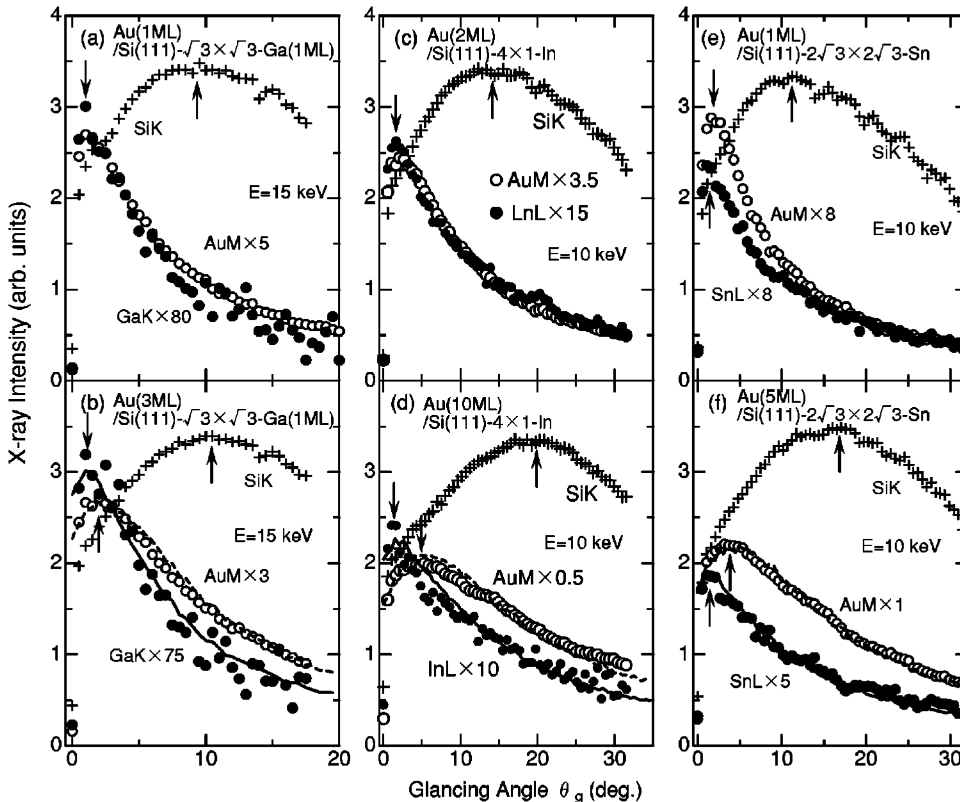

FIG. 4. (a) and (b), (c) and (d), and (e) and (f) show θ_g dependencies of characteristic x-ray emission during growth of Au on Si(111)-$\sqrt{3}\times\sqrt{3}$-Ga (1 ML), 4×1-In and $2\sqrt{3}\times 2\sqrt{3}$-Sn surfaces at room temperature, respectively. Values of Θ_{Au} are indicated in the figures. Solid and dashed curves are θ_g dependencies calculated by Monte Carlo simulation. In the calculation, model (a) in Fig. 6 was assumed for the Au/Ga system, while model (b) in Fig. 6 was assumed for Au/In and Au/Sn systems.

$\sqrt{3}\times\sqrt{3}$-Ga (1 ML) shown in Figs. 2(a) and 2(b). That is, after deposition of 1 ML of Au, shapes of θ_g dependencies of AuM and those of GaK, InL, and SnL were very similar, as shown in Figs. 4(a), 4(c), and 4(e), respectively. After further deposition of Au, the peak positions of AuM shifted to higher θ_g compared with those of GaK, InL, and SnL, as shown in Figs. 4(b), 4(d), and 4(f), respectively. In all of the three growth processes, broad peaks of SiK also sifted to higher θ_g with increases in Θ_{Au}.

IV. DISCUSSION

A. Growth morphology

It is well known that Ag is adsorbed at the initial stage of growth of Ag on an Si(111)-7×7 surface at room temperature, resulting in the formation of clusters at the faulted part of 7×7 unit cells,[14,15] and that larger islands are formed at higher coverages of Ag.[16,17] The formation of islands is clearly indicated by transmitted spots in RHEED patterns.[16,17] Growth of Au on an Si(111)-7×7 surface was studied extensively.[18–38] Although the grown Au film is rather flat at high Au coverage,[38] at the initial stage of this growth the formation of fine particles was observed by scanning tunneling microscopy (STM) images,[18] and RHEED patterns showed weak transmitted spots characteristic of island formation.[39]

On the other hand, during the growth of Ag and Au on $\sqrt{3}\times\sqrt{3}$-Ga (1 ML), $2\sqrt{3}\times2\sqrt{3}$-Sn, and 4×1-In surfaces, RHEED patterns showed streaks but transmitted spots were not observed as shown in Figs. 1(a)–1(f). This means that the grown films were smooth, and that the growth mode was altered from an island growth mode to a layer-by-layer mode by preadsorption of Ga, In, and Sn. This is similar to surfactant-mediated epitaxy, where in the growth of a semiconductor on a semiconductor surface such as Si/Ge and Ge/Si,[1,2] the growth mode is altered from an island growth mode to a layer-by-layer growth mode by preadsorption of small amounts of various elements. In the present study, it was expected that segregation of preadsorbed metals to the uppermost layers or intermixing between preadsorbed metals and grown metals would occur during growth if preadsorbed metals act as surfactants.

B. Atomic depth distribution

In the present study, θ_g dependencies of characteristic x rays from adsorbed metals and SiK showed different behaviors. In addition, these dependencies changed as the coverage of grown metals increased. This is because the θ_g dependence changes according to the depths of elements. By using these phenomena, atomic depth distribution can be analyzed from θ_g dependence of characteristic x rays. Figure 5 shows θ_g dependencies of characteristic x-ray emissions from various layers in a 15-ML Ag film on an Si surface calculated by the Monte Carlo method[40,41] for an incident electron energy of 15 keV. The details of calculation were described in a previous paper.[7] The θ_g dependence calculated for each layer has a maximum, and the position of the maximum shifts to higher θ_g as the depth of the layer increases. The experimental results of θ_g dependence can be explained as a summation of contributions from specific layers.

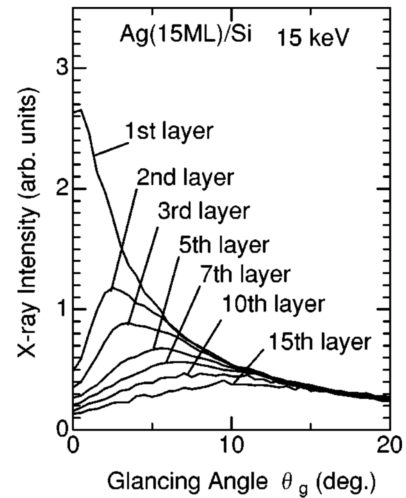

FIG. 5. θ_g dependencies of characteristic x-ray emissions from various layers in a 15-ML Ag film on an Si surface calculated by the Monte Carlo method for an incident electron energy of 15 keV. The position of maximum shifts to higher θ_g as the depth of layer increases.

In the present study, RHEED patterns showed streaks, as can be seen in Fig. 1, indicating the formation of flat films. Therefore, atomic depth distributions were analyzed assuming that the films were flat. In the growth of Ag on a $\sqrt{3}\times\sqrt{3}$-Ga (1 ML) surface, both GaK and AgL had peaks at 1° at $\Theta_{Ag}=1$, as shown in Fig. 2(a). This means that intermixing between Ga and Ag occurred. At $\Theta_{Ag}=3$, GaK showed a peak at 1° but the peak of AgL had shifted to 2°, as shown in Fig. 2(b). This means that segregation of Ga to the uppermost layer had started. At $\Theta_{Ag}=15$, GaK still showed a peak at 1°, while the peak of AgL had shifted to 3°, and the θ_g dependence for GaK decreased more quickly than that for AgL, indicating the segregation of Ga to uppermost layers. Based on these results, the growth model of either (a) or (b) shown in Fig. 6 is proposed. Results of more detailed analyses in order to distinguish these two models are shown in Sec. IV C.

In the growth of Ag on a 1×4-In surface, the θ_g dependencies of AgL and InL were very similar at $\Theta_{Ag}=1$ and $\Theta_{Ag}=6$, as shown in Figs. 3(a) and 3(b), indicating intermixing between Ag and In. Thus, growth model (c) in Fig. 6 is proposed. Similarly, in the growth of Ag on a $2\sqrt{3}\times2\sqrt{3}$-Sn surface, the shapes of θ_g dependencies of SnL and AgL at $\Theta_{Ag}=5$ were very similar, as shown in Fig. 3(c), and therefore growth model (c) in Fig. 6 is proposed for this growth. A similar alloying growth mode was previously observed in the growth of Ga on a Si(111)-$2\sqrt{3}\times2\sqrt{3}$-Sn surface at room temperature.[42]

Similarly, the θ_g dependencies of x-ray emission for the growth of Au on $\sqrt{3}\times\sqrt{3}$-Ga (1 ML), 4×1-In, and $2\sqrt{3}\times2\sqrt{3}$-Sn surfaces shown in Figs. 4(a)–4(f) indicate the segregation of Ga, In and Sn to the uppermost layers, and either growth model (a) or (b) in Fig. 6 is proposed.

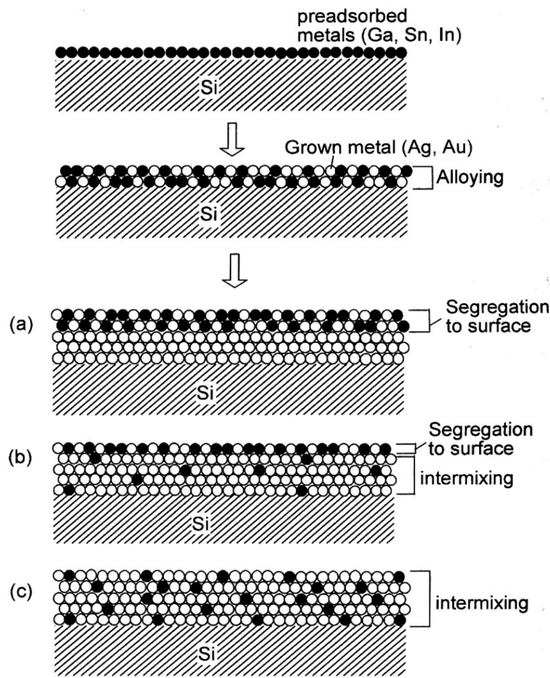

FIG. 6. Growth models of Ag and Au on Si(111)-$\sqrt{3}\times\sqrt{3}$-Ga (1 ML), 4×1-In, and $2\sqrt{3}\times2\sqrt{3}$-Sn surfaces at room temperature. Three kinds of growth modes are proposed depending on the degree of segregation of preadsorbed metals to the uppermost layers. (a) is proposed for Ag/Ga and Au/Ga systems. (b) is proposed for Au/In and Au/Sn systems. (c) is proposed for Ag/In and Ag/Sn systems.

The growth mode of Ag observed in the present work differed from that of Ag on Si(111)-$\sqrt{3}\times\sqrt{3}$-Au, where Ag grows on an Au layer. The latter may be due to the bonding energy of Au-Si,[43] which is higher than the energy of Ag-Si bonding.[43] However, it seems difficult to explain the mechanism of site exchange only from the binding energy. For example, in the present study, dissociation of Ga occurred when Ag was deposited on a Si(111)-$\sqrt{3}\times\sqrt{3}$-Ga (1 ML) surface, but in previous studies dissociation of Ag was induced by Ga deposition on an Si(111)-$\sqrt{3}\times\sqrt{3}$-Ag surface.[42,44]

During growth of Au on a Si(111)-7×7 surface, formation of particles was observed around $\Theta_{Au}=3$ in an STM study,[18] and RHEED patterns during this growth showed weak transmitted spots characteristic of particles.[39] However, at high Θ_{Au}, some Si atoms segregate to the uppermost layers resulting in the formation of Au-Si silicide layers,[36] and the resultant Au film is flat.[38] Thus, at high Θ_{Au}, floating Si may act as a surfactant. In the growth of Au on the three metal-covered Si(111) surfaces, the possibility of existence of surface silicide layers could not be ruled out by analysis of RHEED patterns and θ_g dependencies, and Si may exist in the uppermost layers at high Θ_{Au} and act as a surfactant. However, the Au films grown on the three metal-covered surfaces are flatter than is a Au film directly grown on a Si(111)-7×7 surface, since RHEED patterns during growth of Au on the three metal-covered surfaces did not show any transmitted spots, as can be seen in Figs. 1(d)–1(f). Thus the surfactant effects of Ga, In, and Sn are also significant. The results of the present study indicate that the surfactant effect in the growth of metals on metal-covered semiconductor surfaces is a general phenomenon.

Many different growth modes have been observed in other metal/metal/Si(111) systems at room temperature. In the growth of In on Si(111)-$\sqrt{3}\times\sqrt{3}$-Ga (1 ML),[4–6] Ga acts as a surfactant and always exists at the third layer.[4] In the growth of Au on $\sqrt{3}\times\sqrt{3}$-Ag, substitution between Ag and Au occurs after 1 ML of Au deposition, resulting in the formation of Ag particles on a Au layer.[7] With further deposition of Au, Ag clusters still exist in the upper parts of the grown film. In the growth of Ga on $\sqrt{3}\times\sqrt{3}$-Ag,[42,44] site exchange between Ga and Ag occurs after 1 ML of Ga deposition, resulting in the formation of Ag particles and a Ga underlayer. During further Ga deposition, Ga surrounds the Ag particles. These results indicate that there are various possibilities for controlling the morphology of grown films by preadsorption of other atoms, and control of the morphology would be useful for fabricating and studying nanostructures with new functions. However, a high degree of thermal stability of grown films is required for the actual application of such films to device technology, and it may not be easy to obtain a high degree of thermal stability of such films.

C. Analysis by the Monte Carlo method

In the growth processes of Ag/$\sqrt{3}\times\sqrt{3}$-Ga (1 ML), Au/$\sqrt{3}\times\sqrt{3}$-Ga (1 ML), Au/4×1-In, and Au/$2\sqrt{3}\times2\sqrt{3}$-Sn systems, segregation of preadsorbed metals to the uppermost layers was observed, and growth modes in these processes are thought to be either (a) or (b) in Fig. 6. To distinguish these two models, we tried to fit the experimental results with theoretical curves calculated by Monte Carlo simulation.

There are two kinds of fitting parameters. One is distribution of elements. For Ag/$\sqrt{3}\times\sqrt{3}$-Ga (1 ML), it was assumed that 0.25 ML of Ga is uniformly distributed in each of the first to the fourth layers at $\Theta_{Ag}=15$ ML, resulting in total Ga coverage of 1 ML [growth model (a) in Fig. 6]. The other is the detection probability of x rays as a function of depth, which decreases when the position of x-ray emission becomes deeper due to absorption and refraction. Under the TRAXS condition, x rays emitted from shallow regions, where evanescent waves exist in total reflection, are detected. However, in the present measurements, the window of the detection angle contained the total reflection angle and also angles slightly higher than the total reflection angle to observe x rays from deeper regions. In this case, as the energy of the x rays increases, the depth of the evanescent wave from the surface decreases, but the penetration length of the x rays increases. In this analysis, it was assumed that x-ray intensities decrease by a factor of 0.95 as the depth of the layer increases by 1 ML, independent of the x-ray energy. This value induces increment of the ratio of AgL relative to SiK by 25 times when the Ag coverage increases from 1 to 15 ML at high θ_g, assuming the above depth distribution of Ag and Ga. This is roughly consistent with the experimental results shown in Figs. 2(a) and 2(c), where the relative ratio increases by 28 times at 20°. The value of 0.95 corresponds

to the depth of depletion length (23 Å) of evanescent waves of x rays with an energy of about 0.55 keV. This depletion length is longer than those of evanescent waves of SiK (7.1 Å, 1.74 keV), AgL (4.1 Å, 3 keV) and GaK (1.3 Å, 9.2 keV), and it is therefore thought that the detection angle of the x ray was higher than the total reflection angle. One possible fitting is shown by solid and dashed curves in Fig. 2(c). Both experimental results for GaK and AgL are explained well by the simulated curves.

A growth model similar to that of growth model (a) in Fig. 6 was proposed for the growth of Au on a $\sqrt{3}\times\sqrt{3}$-Ga (1 ML) surface. It was assumed that 2/3 ML and 1/3 ML of Ga exist in the first and second layers, respectively. In this analysis, the depletion factor of x-ray was assumed to be 0.79. This value is smaller than the value of 0.95 used for Ag/$\sqrt{3}\times\sqrt{3}$-Ga (1 ML), which may result from differences in detection angles, penetration lengths and refractive indices of x rays in Ag and Au. The value of 0.79 corresponds to the depth of depletion length (5.16 Å) of evanescent waves of x rays with energy of about 2.4 keV, which is in the same order as the energy of characteristic x rays detected in the present work [1.74 keV (SiK), 2.2 keV (AuM), 3.2 keV (InL), 3.3 keV (SnL) and 9.2 keV (GaK)]. This value should induce an increment of the ratio of AuM relative to SiK by 3.5 times when the Au coverage increases from 1 to 3 ML at high θ_g, assuming the above depth distribution of Au and Ga. This is roughly consistent with the experimental results shown in Figs. 4(a) and 4(b), where the relative ratio increases by 2.8 times at 30°. One possible fitting is shown by solid and dashed curves in Fig. 4(b). Experimental results for both GaK and AuM are explained well by the simulated curves.

For the growth processes of Au on 4×1-In and $2\sqrt{3}\times2\sqrt{3}$-Sn surfaces, both segregation of preadsorbed metals to the uppermost layers and intermixing between preadsorbed and grown metals had to be assumed to obtain good fitting results, and growth model (b) in Fig. 6 was proposed. The results are shown by solid and dashed curves in Figs. 4(d) and 4(f). For Au/4×1-In, it was assumed that 0.22 ML of In exists in the first layer and that each of the second to eleventh layers contains 0.078 ML of In, resulting in 1 ML of total amount of In atoms, and the depletion factor was 0.79. This value should induce increment of the ratio of AuM relative to that of SiK by about 12 times when Au coverage increases from 2 ML to 10 ML, which is close to the observed increment, about ten times, as shown in Figs. 4(c) and 4(d), at 30°. For a Au/$2\sqrt{3}\times2\sqrt{3}$-Sn surface, it was assumed that 0.4 ML of Sn exists in the first layer and that each of the second to sixth layers contains 0.12 ML of Sn, resulting in 1 ML of total amount of Sn atoms, and the depletion factor of x rays was assumed to be 0.79. This value should induce increment of the ratio of AuM relative to SiK by eight times when the Au coverage increases from 1 to 5 ML at high θ_g, assuming the above depth distribution of Au and Sn, which is consistent with the experimental results shown in Figs. 4(e) and 4(f), where the relative ratio increases by nine times at 30°.

From the results of the above fitting, growth model (a) in Fig. 6 was proposed for Ag on $\sqrt{3}\times\sqrt{3}$-Ga (1 ML) and Au on $\sqrt{3}\times\sqrt{3}$-Ga (1 ML), and model (b) in Fig. 6 was proposed for Au on 4×1-In and Au on $2\sqrt{3}\times2\sqrt{3}$-Sn. Since only simple distributions of elements were assumed in the present fitting, the fitting may improve if more detailed distributions of elements are assumed.

V. SUMMARY

Growth modes of Ag and Au on three surfaces, Si(111)-$\sqrt{3}\times\sqrt{3}$-Ga (1 ML), 4×1-In, and $2\sqrt{3}\times2\sqrt{3}$-Sn surfaces, at room temperature were studied by RHHED and characteristic x-ray measurements as functions of incident glancing angle of the electron beam. In all growth processes, intermixing between preadsorbed metals (Ga, In, In, metal A) and grown metals (Au, Ag, metal B) occurred after deposition of 1 ML of metal B. During further deposition, segregation of metal A to the uppermost layers occurred in the Ag/Ga and Au/Ga systems, while further intermixing between metals A and B was observed in the Ag/In and Ag/Sn systems. In the Au/In and Au/Sn systems, partial segregation of metal A and partial intermixing between metals A and B were observed. The roughness of Ag and Au films was suppressed by preadsorbed metals, resulting in the formation of flat films. These results suggest that the surfactant effect of a preadsorbed metal on metal growth on Si surfaces is a general phenomenon.

---

*Corresponding author. Electronic mail: yama@cat.hokudai.ac.jp

[1] M. Copel, M.C. Reuter, E. Kaxiras, and R.M. Tromp, Phys. Rev. Lett. **63**, 632 (1989).

[2] M. Horn-von Hoegen, F.K. LeGoues, M. Copel, M.C. Reuter, and R.M. Tromp, Phys. Rev. Lett. **67**, 1130 (1991).

[3] H.A. van der Vegt, H.M. van Pinxteren, M. Lohmeier, E. Vlieg, and J.M.C. Thornton, Phys. Rev. Lett. **68**, 3335 (1992).

[4] T. Yamanaka and S. Ino, Jpn. J. Appl. Phys. **35**, 3991 (1996).

[5] N. Shimomura, T. Yamanaka, and S. Ino, Jpn. J. Appl. Phys. **34**, 6201 (1995).

[6] T. Yamanaka, N. Shimomura, and S. Ino, Surf. Sci. **356**, 39 (1996).

[7] T. Yamanaka, A. Endo, and S. Ino, Surf. Sci. **294**, 53 (1993).

[8] R.S. Becker, J.A. Golovchenko, and J.R. Patel, Phys. Rev. Lett. **50**, 153 (1982).

[9] S. Hasegawa, S. Ino, Y. Yamamoto, and H. Daimon, Jpn. J. Appl. Phys. **24**, L387 (1985).

[10] T. Yamanaka and S. Ino, Rev. Sci. Instrum. **72**, 1477 (2001).

[11] J. Zegenhagen, J.R. Patel, P. Freeland, D.M. Chen, J.A. Golovchenko, P. Bedrossian, and J.E. Northrup, Phys. Rev. B **39**, 1298 (1989).

[12] J. Nogami, S-I. Park, and C.F. Quate, Phys. Rev. B **36**, 6221 (1987).

[13] T. Ichikawa, Surf. Sci. **140**, 37 (1984).

[14] St. Tosch and H. Neddermeyer, Phys. Rev. Lett. **61**, 349 (1988).

[15] H. Neddermeyer, Solid State Mater. Sci. **16**, 309 (1990).

[16] Y. Gotoh and S. Ino, Jpn. J. Appl. Phys. **12**, 2097 (1978).

[17] Y. Gotoh and S. Ino, Thin Solid Films **109**, 255 (1983).

[18] I. Chizhov, G. Lee, and R.F. Willis, Phys. Rev. B **56**, 12316 (1997).

[19] G. Le Lay and J.P. Faurie, Surf. Sci. **69**, 295 (1977).
[20] L. Braicovich, C.M. Garner, P.R. Skeath, C.Y. Su, P.W. Chye, I. Lindau, and W.E. Spicer, Phys. Rev. B **20**, 5131 (1979).
[21] K. Okuno, T. Ito, M. Iwami, and A. Hiraki, Solid State Commun. **34**, 493 (1980).
[22] P. Perfetti, S. Nannarone, F. Patella, C. Quaresima, M. Capozi, A. Savoia, and G. Ottaviani, Phys. Rev. B **26**, 1125 (1982).
[23] T. Ito and W.M. Gibson, J. Vac. Sci. Technol. A **2**, 561 (1984).
[24] A. Taleb-Ibrahimi, C.A. Sebenne, D. Bolmont, and P. Chen, Surf. Sci. **146**, 229 (1984).
[25] R. Cao, J.-J. Yeh, J. Nogami, and I. Lindau, J. Vac. Sci. Technol. A **4**, 846 (1986).
[26] S.M. Durbin, L.E. Berman, and B.W. Batterman, Phys. Rev. B **33**, 4402 (1986).
[27] J.-J. Yeh, J. Hwang, R. Cao, K.A. Bertness, and I. Lindau, J. Vac. Sci. Technol. A **6**, 1557 (1988).
[28] M. Iwami, T. Terada, H. Tochihara, M. Kubota, and Y. Murata, Surf. Sci. **194**, 115 (1988).
[29] S.L. Molodtsov, C. Laubschat, G. Kaindl, A.M. Shikin, and V.K. Adamchuk, Phys. Rev. B **44**, 8850 (1991).
[30] S.L. Molodtsov, C. Laubshat, A.M. Shikin, and V.K. Adamchuk, Surf. Sci. **269/270**, 988 (1992).
[31] K. Meinel and D. Katzer, Appl. Surf. Sci. **56-58**, 514 (1992).
[32] J.-J. Yeh, J. Hwang, K. Bertness, D.J. Friedman, R. Cao, and I. Lindau, Phys. Rev. Lett. **70**, 3768 (1993).
[33] M.T. Cuberes, A. Bauer, H.J. Wen, D. Vandre, M. Prietsch, and G. Kaindl, J. Vac. Sci. Technol. B **12**, 2422 (1994).
[34] M. Schleberger, D. Fujita, C. Scharfschwerdt, and S. Tougaard, Surf. Sci. **331-333**, 942 (1995).
[35] K.N. Tu, Appl. Phys. Lett. **27**, 221 (1975).
[36] A. Hiraki, Surf. Sci. Rep. **3**, 357 (1984).
[37] D. Katzer and K. Meinel, J. Cryst. Growth **98**, 690 (1989).
[38] H. Okamoto and H. Nejo, J. Vac. Sci. Technol. B **16**, 3013 (1998).
[39] N. Shimomura, Ph.D. thesis, University of Tokyo, 1996.
[40] K. Murata, T. Matsukawa, and R. Shimizu, Jpn. J. Appl. Phys. **10**, 678 (1971).
[41] D.E. Newbury, in *Advanced Scanning Electron Microscopy and X-ray Microanalysis*, edited by D.E. Newbury, D.C. Joy, P. Echlin, C.E. Fiori, and J.I. Goldstein (Plenum, New York, 1986), p. 3.
[42] T. Yamanaka and S. Ino, Surf. Sci. **330**, 126 (1995).
[43] G. LeLay, M. Manneville, and R. Kern, Surf. Sci. **65**, 265 (1977); **72**, 405 (1978).
[44] T. Yamanaka, N. Shimomura, and S. Ino, Appl. Phys. Lett. **77**, 3983 (2000).